

# Oxide Layers Growth on AISI 1006 Steel through ‘Asymmetric Bipolar Pulsed Plasma’ Process

Paula Fin<sup>a</sup>, Abel A. C. Recco<sup>a</sup> , Juliano Sadi Scholtz<sup>a</sup>, Luis C. Fontana<sup>a,\*</sup> 

<sup>a</sup>Universidade do Estado de Santa Catarina, Departamento de Física, R. Paulo Malschitzki, 200, Zona Industrial Norte, 89219-710, Joinville, SC, Brasil.

Received: September 18, 2021; Revised: December 16, 2021; Accepted: January 12, 2022

The main problem in metal oxidation is the spalling and de-cohesion of the oxide layer, which results in delamination due to strong compressive stress gradient through the layer. Present paper proposes the use of a modified process named Asymmetric Bipolar Pulsed Plasma (ABiPPS) for plasma-oxidation treatment of low carbon steel AISI-1006 samples. Results show that the ABiPPS process ensures high plasma stability and enables the growth of uniform oxide layers (with thickness up to 6  $\mu\text{m}$ ) on metal surfaces. Plasma generated through bipolar asymmetric voltage pulses provides better control on surface bombardment through interspersed jets of ions and electrons, during the oxidation process. The control of intermittent ions and electrons bombardment (through voltage peaks up to 1.5 kV and period about 1  $\mu\text{s}$ ), during plasma oxidation, make it possible to improve the adhesion between the oxide layer and the substrate, moreover the control of crystalline phases, such as hematite and magnetite.

**Keywords:** *oxide layer, asymmetric bipolar pulsed plasma ABiPPS, ion and electron bombardment.*

## 1. Introduction

Low temperature plasma (LTP) has been successfully used for surface treatments, such as plasma nitriding and plasma carburizing. However, little attention has been paid to plasma oxidation, which may improve surface properties such as corrosion resistance and hardness. In addition, oxide layers can be used as insulating surfaces in electrical, electronic, and optoelectronic devices. Iron oxides are used in a wide array of applications such as corrosion protective coatings, catalysis, spintronics, magnetic nanoparticles (MNPs), biomedicine, photoelectrochemical water splitting and groundwater remediation. Due to their low toxicity, stability, and economic viability, make them ideal for application in a wide range of emerging fields<sup>1</sup>.

Iron oxide can exist in several phases, the three main phases are magnetite, hematite and maghemite. The basic distinguishable properties of iron oxide phases are the magnetic and the electrical behavior<sup>2</sup>, which make the applications directly related to the oxide phases.

Surface oxidation of metals are often damaged by spalling and de-cohesion of the oxide layers. The spalling and de-cohesion are consequences of the growth strain associated to the formation of the oxide layer on substrate. The possible origins for the growth strain are the following: incompatibility of the crystalline lattices between the oxide layer and the substrate; incompatibility of the molar volumes; possibility that the oxide growth in the oxide grain boundary leads to a compression stress state in this layer<sup>3</sup>. Rhines–Wolf model<sup>4</sup> have established that the associated stresses cannot be due to incompatibilities at the metal/oxide interfaces or along grain boundaries parallel to these interfaces. These

authors propose that only oxide growth along grain boundaries, lying perpendicular to the interface, generate a lateral strain, concomitantly to inward diffusion of oxygen and outward diffusion of metal ions. Therefore, the microstructure and diffusion are important factors on the oxide layer stress. Clarke model<sup>5</sup> improved the Rhines–Wolf model for the lateral strain rate accompanying the growth of an oxide is developed based on trapping of counter-diffusing cations and anions at the core of edge dislocations causing them to climb through the oxide thickness. The Clarke model also predicts that the lateral growth strain rate increases linearly with the oxide thickening. Panicaud et al.<sup>6</sup> proposes a model to predict the evolution of the residual stresses in the growing oxides layers, during isothermal high temperature oxidation. They assume a proportional dependence of the growth strain with the oxide layer thickness, so they use a system of equations that predict the stresses evolution with oxidation time. The model consider diffusion in the grain boundaries and consider both the growth strain term and the relaxation phenomena. The macroscopic growth strain follows the kinetic evolutions of the oxide layer thickness. The equations proposed by Panicaud et al.<sup>6</sup>, consider two main parameters: on the one hand the parameter  $D$  ( $\text{m}^{-1}$ ) which influences the oxidation process and generate a significant evolution of the lateral growth strain; on the other hand, the creep parameter  $J$  ( $\text{Pa}^{-1} \text{s}^{-1}$ ) dominates the relaxation of stresses in the oxide layer, which indicates a decreasing regime of stress after a maximum value has been attained. The oxide tends to expand laterally but suffer substrate constraints, which produces compressive stress in the plane of the oxide layer and a corresponding tensile stress on the substrate itself. So, the spalling and de-cohesion take place generally at interface due

\*e-mail: [luis.fontana@udesc.br](mailto:luis.fontana@udesc.br)

to the stress between substrate and oxide layer. As reported above, the oxide/metal system has a growth strain term and the relaxation phenomena, related through respectively the parameters  $D_{ox}$  and  $J$ . Therefore, these parameters depend on the thermodynamics and the diffusion of atoms (inward or outward). Based on the above explanation, we propose a modified methodology to produce more adherent oxide layer on low carbon steel. The proposition consists of promoting interspersed ionic/electronic bombardment on sample surface, during the oxidation through asymmetric bipolar pulsed plasma (ABiPPS). Since the ABiPPS oxidation process allows to control the energy delivered to surface during the treatment, it could control of stress and creep kinetics in the oxide layer.

A variety of methods have been used to produce oxide layers on metal substrate such as plasma electrolytic oxidation (PEO), Radio frequency plasma (RFP) and pulsed plasma. Nowadays, PEO is the most studied process for metal oxidation. However, PEO process presents some issues as high porosity of the oxide layer formed on the surface and high-energy consumption<sup>7</sup>. Low-pressure RF plasma has also been used for metal oxidation; however, this process is most suitable for thin oxide films in semiconductor manufacturing processes<sup>8,9</sup>. The use of DC discharge for surface oxidation, through plasma, is not suitable due to the insulating oxide layer growth on the piece surface, which can produce plasma arcing and make it difficult to maintain the plasma discharge, besides produces damage on surfaces being treated<sup>10</sup>.

This paper proposes a new technique for low-pressure plasma oxidation which consists of a modified voltage waveform for plasma generation, named Asymmetric Bipolar Plasma Power Supply (ABiPPS). The bipolar pulsed voltage, composed of intense positive and negative pulses as short as 1  $\mu$ s, allows the surface to be sequentially hit by ion and electron bombardments, which, consequently, significantly increases the plasma ionization rate due to high secondary electrons emission from electrode<sup>11</sup>. In addition, the bombardment interspersed with ions and electrons make possible the plasma maintenance, despite the surface becoming an insulator (oxide layer).

The electronic/ionic bombardment can heat the work piece in a controlled manner and may activate both, chemical reactions, and diffusion of atoms on surface, providing better control in the oxide layers growing<sup>12</sup>. In turn, the electron bombardment has a pivotal role on chemical reactions in condensed matter<sup>13</sup>. For example, the electron impact has been shown to enhance the oxidation of Si (100) and form a thick film of silicon dioxide<sup>14</sup>. The ion/electron energy distribution (IED/EED) may be controlled by tuning the intensity and the period of voltage pulses. In this way, a pulsed power supply may allow an ion/electron energy most suitable to promote heating, diffusion, and electron-induced reactions on substrate surface<sup>15</sup>. Consequently, it may be possible to control the growing kinetics of the oxide layers through the ion/electron bombardment, during the treatment.

This paper aims to investigate the growing of cohesive oxide layers on low carbon steel AISI 1006 through Asymmetric Bipolar Pulsed Plasma (ABiPPS) technique. The ABiPPS system provides flexibility to control the voltage waveform and the intensity of voltage pulses, so it makes possible the

control of the energy delivered to surface through electronic and ionic bombardment. Consequently, the use of ABiPPS plasma power supply for metal oxidation may render feasible the control of both phenomena predicted by Panicaud et al.<sup>6</sup>: the kinetic of growth strain and relaxation phenomena.

## 2. Experimental Details

Samples of AISI 1006 steel were oxidized through plasma generated by ABiPPS process. The chemical composition of low carbon AISI 1006 steel samples used in this work is the following: Fe (99.43-99.75%); C (0.08% max); Mn (0.35% max); P (0.04% max); S (0.05% max). Samples were treated at different time and temperature, namely: 2.0h and 0.5h; 300°C (573K) and 500°C (773K). Prior to the treatment, the samples were polished (with alumina 1,0  $\mu$ m) and cleaned in ultrasound (with isopropanol) during 10 min. The final pressure into the vacuum chamber was 1,3 Pa, and the treatment was carried out in oxygen plasma (99.999%) at working pressure of 67 Pa. Figure 1A shows the schematic experimental apparatus and special focus was placed on the waveform voltage provided by an ABiPPS power supply.

The bottom of Figure 1 illustrates the interspersed bombardment of electrons and ions hitting the electrode, at different voltage values provided by the ABiPPS power supply: (B1) illustrates the electrode (e. g., the piece to be treated) biased during positive voltage peak, when it is bombarded by energetic electrons and by possible negative ions of oxygen; (B2) illustrates the electrode bombardment by positive ions, during intense negative voltage pulse; (B3) illustrates the electrode being bombarded by low energy positive ions during longer period negative lower voltage. This voltage pulse waveform promotes the bombardment of the electrode by high energy electrons, high energy ions and lower energy ions. Table 1 shows the values of period and voltage peaks used in this work. The adjustment of those variables' values allows the adjustment of the average temperature of the samples at 300°C and 500°C (573 K and 773K). The temperature measurement was performed through a thermocouple attached to a standard sample.

## 3. Results and Discussions

Figure 2a shows the surface of a sample treated at 500°C for 2h (O500-2). The picture shows that the oxide layer was almost completely detached from the surface. Figure 2b shows the cross section of a region where the oxide layer was not detached. It is possible to notice in region I, pointed on the Figure 2b, one of the transverse cracks in the layer. The region II indicates a non-cohesive layer, where it is possible to see a crack between the layer and the substrate. According to Panicaud et al.<sup>6</sup>, the oxide tends to expand laterally but suffers substrate constraints, which produces compressive stress in the plane of the oxide layer and a corresponding tensile stress on the substrate itself, as the film thickness increases. So, the spalling and de-cohesion take place generally at interface due to the stress between substrate and oxide layer. Figure 2c and Figure 2d show the surface and the cross-section, respectively, of a sample treated in low temperature and short time, namely 300°C and 0.5h. It is not observed any detachment on surface. In fact,

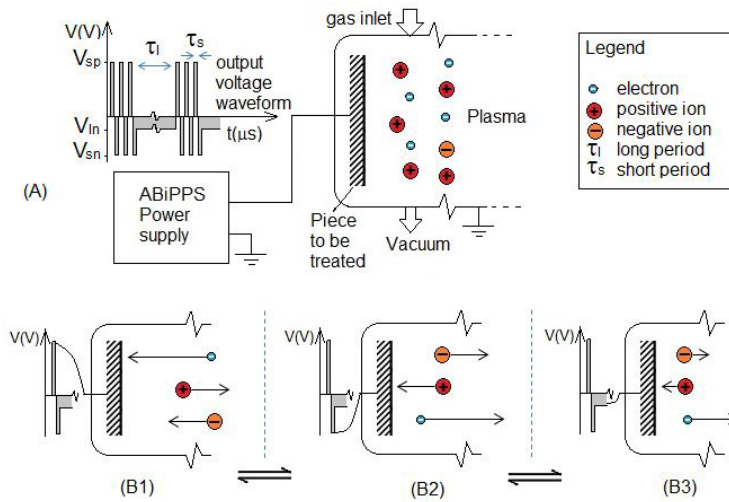


**Figure 1.** (A) Voltage waveform provided by ABiPPS power supply connected to the samples during the plasma oxidation. (B) forces experienced by electrons and ions in different point-in-time on voltage waveform graphics: (B1) high positive voltage, so negative charge carriers (electrons and negative ions) are accelerated toward the electrode (samples); (B2) negative high voltage, so positive ions are accelerated toward the electrode; (B3) lower negative voltage (during longer time), so positive ions hit the electrode with mild mean energy.

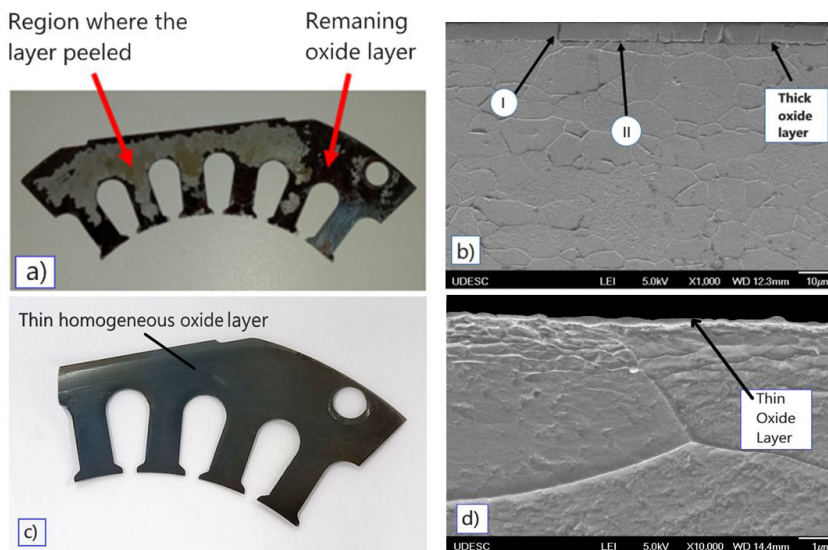


**Figure 2.** Samples treated under unfavorable condition for generation of homogeneous, thick, and adherent oxide layers. Sample (O500-2h) treated at 500°C for 2,0h: a) detached layer region; b) cross section micrography showing spalling and de-cohesion at interface layer-core. Sample (O300-0,5h) treated at 300°C for 0,5h: c) homogeneous surface after oxidation; d) cross section indicating non-formation of a well-defined oxide layer.

**Table 1.** Oxidation parameters and the resulting oxide layers thickness. Legend: -Vsn /-Vln / +Vsp (short-negative / long-negative / short-positive voltage peaks); τs / τl (short time / long time)

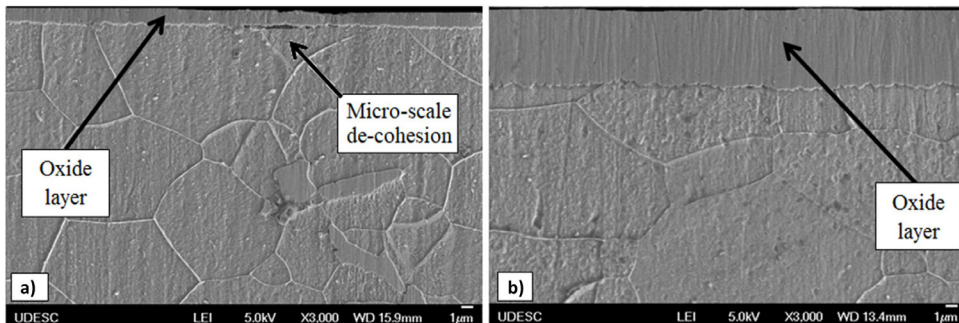
Sample name	Treatment Time (h)	Temp. (°C)	ABiPPS parameters					Resulting oxide layer (thickness)
			Voltage peaks (V)			Peak Period (μs)		
			-Vsn	-Vln	+Vsp	τs	τl	
O300-0.5	0.5	300	1000	360	600	1.0	10.0	>0.2 μm
O300-2	2.0							1.0±0.2 μm
O500-0.5	0.5	500	1350	500	600	1.0	10.0	6.0±0.2 μm
O500-2	2.0							spalling layer

Figure 2d indicate that the region next to the surface was changed but it is not possible identify any well-defined oxide layer generation. On the other hand, different combinations of time/temperature parameters (e. g. "O300-2" and "O500-0.5" samples) can produces more homogeneous and better adherent oxide layers through ABiPPS plasma process, as it will be shown below.

Figure 3a and 3b show cross section scanning electron microscopy (SEM) images of samples treated under more suitable parameters combination. The samples O300-2 and O500-0.5 shown homogeneous and more adherent oxide layers. The samples treated in those conditions do not shown spalling of the oxide layers. Samples treated in low temperature, 300°C for a period of 2.0h (O300-2) show uniform thickness about  $1.1 \pm 0.2 \mu\text{m}$ . Although, macroscopically, the layer appears to be homogeneous and adherent to substrate, it is possible to observe some micro-scale de-cohesion evidence at metal-oxide interface, as shown in Figure 3a. Samples treated at higher temperature, namely 500°C, for short period of time (0.5h), presented thicker oxide layers, about  $6.4 \pm 0.2 \mu\text{m}$ . Results show uniform and no spalling of oxide layers growth on samples with surface area of

$100 \text{ mm}^2$  (Figure 3b). The residual stress relieving during surface oxidation is the main hypothesis to explain the better cohesion of oxide layer. Such stress relieving is due to the flexibility of process parameters, which enables the control of energy delivered to surface through ions and electrons bombardment, provided by ABiPPS system. Even though a thick layer, it is feasible that the high energy bombardment, through ion/electron, increases the localized temperature at surface. Consequently, the localized heating can accelerate the creep mechanism<sup>6</sup> and so, it promotes further stress relieving in the oxide layer.

Figure 4 shows results of chemical analysis through Energy-Dispersive Spectroscopy (EDS) technique. It is observed high intensity oxygen peaks on the layers, as expected. However, the carbon concentrations in the oxide layers at the two temperatures differ greatly: the carbon concentration in the layer increases for O300-2h sample and decreases for O500-0.5h, if compared to the core substrate. The carbon diffusion, from the core to the surface, is a well-known effect in plasma nitriding process<sup>16</sup>. Considering that the diffusion increases exponentially as the temperature increases, it is reasonable to consider that, at the temperature of 500°C the



**Figure 3.** Cross section images of oxide layers (SEM): a) sample O300-2h; b) sample O500-0.5h.

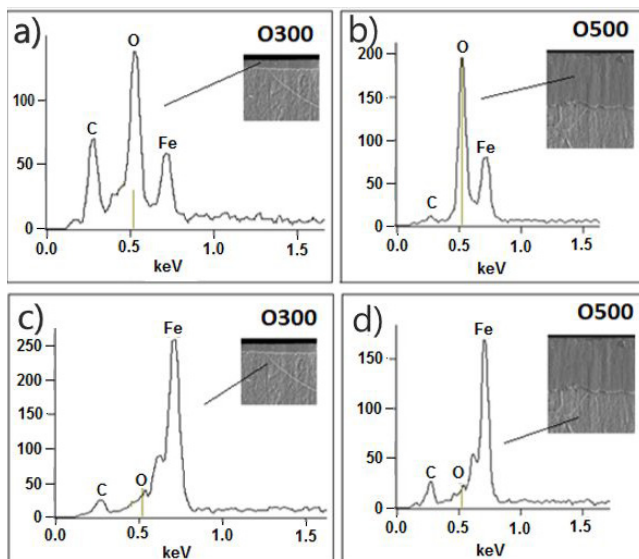


**Figure 4.** EDS results at different positions next to the surface: oxide layers (a, b); below oxide layers (c, d).

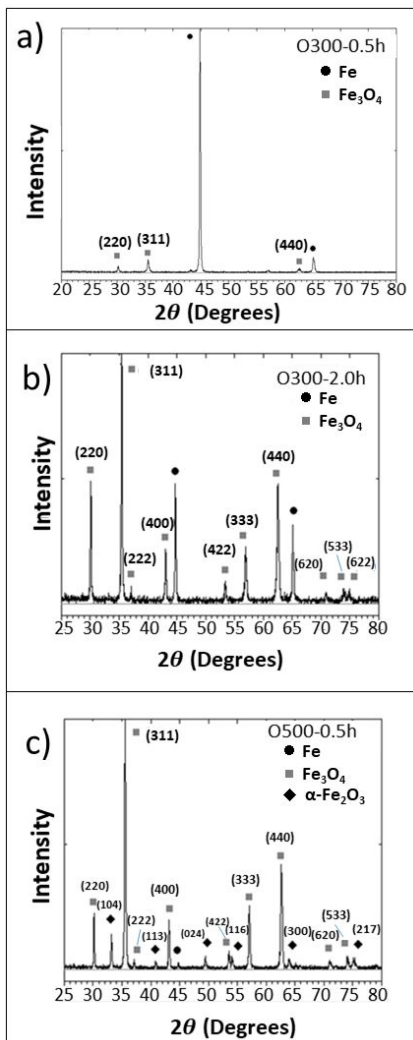
carbon atoms can reach the surface of the sample. Those carbon atoms can react with the oxygen from the plasma, resulting in  $\text{CO}_x$  gas, which can be eliminated through the vacuum pump. At lower temperature ( $300^\circ\text{C}$ ) the carbon diffusion is lower, and the oxide layer acts as a diffusion barrier for carbon atoms, which causes carbon concentration in the layer. Figure 4c, d show traces of oxygen in substrate, below the oxide layers, suggesting that may exist oxygen in solid solution in this region of the samples.

Figure 5 shows the x-ray diffraction (XRD) results for the samples O300-0.5h, O300-2.0h and O500-0.5h. The XRD spectrum from O300-0.5h sample (Figure 5a) shows peaks corresponding to the magnetite phase  $\text{Fe}_3\text{O}_4$  (COD ID 1539747) which present low intensity in comparison to the  $\alpha$ -Fe peak (COD ID 4113928). The magnetite peaks appear in very low intensity due to low thickness of the oxide layer obtained in these conditions of treatment. Figure 5b shows the XRD spectrum from O300-2h sample, where it is identified more intense peaks corresponding to the oxide phase of

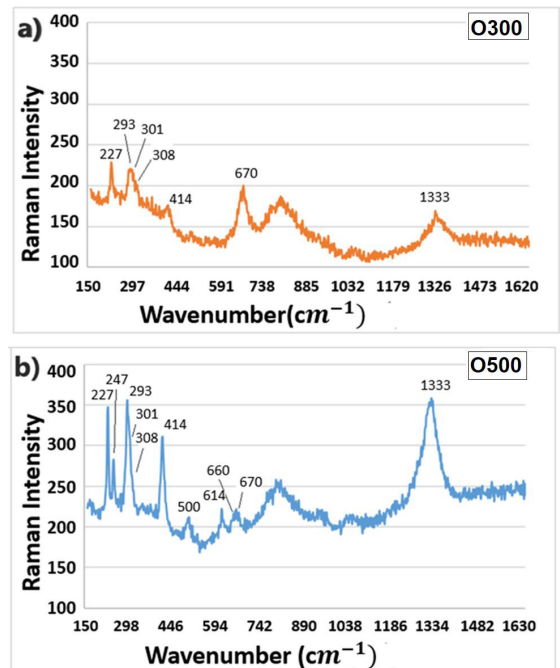
magnetite  $\text{Fe}_3\text{O}_4$  (COD ID 1539747). Some  $\alpha$ -Fe (COD ID 4113928) peaks also appear in the diffraction pattern due to x-ray diffraction in the steel substrate. Figure 5c shows results for O500-0.5h samples, which indicates the formation of two phases: magnetite and hematite  $\alpha\text{-Fe}_2\text{O}_3$  (COD ID 1546383). This XRD spectrum does not show peaks of the substrate due to the great thickness of the oxide layer ( $\sim 6\mu\text{m}$ ). In short, XRD results from thicker films show two oxide phases, namely, magnetite and hematite, whereas XRD from thinner films show only the magnetite phase.

Figure 6 shows Raman spectra from the oxide layers formed at 300 K and 500 K. The spectra for the O300 samples can be assigned to both magnetite and hematite, according to Raman bands at 308 and 670 (characteristic of magnetite) and at 227, 293, 301, 414 and 1333 (characteristic of hematite). In turn, the spectral of O500 samples can be assigned mostly to hematite according to Raman bands at 227, 247, 293, 301, 414, 499, 614, 660 and 1333.

The XRD and Raman analysis show complementary results regarding to oxide layer phases identification. The penetration depth of X-ray beams (Cu K-alpha,  $\lambda=1.541 \text{ \AA}$ ) in Fe-O material is up to  $5 \mu\text{m}$ <sup>17</sup>. In turn, the radiation penetration depth in Raman analysis is less than  $3 \mu\text{m}$  and depends on the material and the LASER wavelength<sup>18</sup>. The XRD analysis of O300 samples shows only magnetite phase, while the Raman measurements show both magnetite and hematite. Therefore, it is probable that there is a thin layer of hematite on the top, detected by Raman analysis, but it does not appear on the XRD analysis due to lesser thickness of the oxide layer. Samples O500 show clearly both phase magnetite and hematite in Raman and XRD characterizations.



**Figure 5.** X-ray diffraction results of following samples: a) O300-0.5h; b) O300-2.0; c) O500-0.5h.



**Figure 6.** Raman spectroscopy analysis: a) samples O300, b) samples O500.

Jonsson et al.<sup>19</sup> reported a similar situation, where magnetite is formed beneath a thin fine-grained hematite layer.

Hardness measurements were carried out on the surface oxide layers, at room temperature, through an instrumented nano-indentation testing using CETR-UMT-02, equipped with a Berkovich Diamond indenter. Figure 7a illustrate a load-vs-displacement curve taken by nanoindentation on surface of an oxidize sample. Figure 7b shows the dwell period at the peak load, which was fixed as 10 s. The test was carried out by applying force on the surface, then releasing and change to a different position, applying the new force with an incremental loading. The analyzing load-depth data was made according to the Oliver and Pharr method<sup>20</sup>. The calibration process to obtain the penetrator area function and the mechanical stiffness (machine compliance) were carried out according to the ISO 14577-1 standard<sup>21</sup>. The loading/unloading cycles were repeated 10 times, with load ranges between 20mN and 120mN. The Poisson's ratios used were 0.37, that correspond to magnetite.

Figure 8a shows the hardness on the oxide layer for the sample O300-2h. The first hardness value, for depth penetration of 0.16  $\mu\text{m}$ , is  $11.0 \pm 0.2$  GPa. For higher penetration depth, the hardness values are highly influenced by the mechanical properties of the substrate. As the oxide layer thickness of O300-2h sample is thin ( $\sim 1$   $\mu\text{m}$ ), the surface hardness begins to have contribution from the substrate early. This contribution starts right after the first indentations and drops steeply at first measurement points. The surface hardness for the sample O500-0.5h is showed in Figure 8b and its

value is  $9.6 \pm 0.2$  GPa for penetration depth around 0.46  $\mu\text{m}$ ; farther, for depths greater than 0.46  $\mu\text{m}$ , the hardness values decrease as the load was increased. The hardness decreases as the depth of penetration increases because more of the hardness contribution will arise from the substrate<sup>22</sup>.

The hardness values for iron oxides found in the literature vary between 5.88 and 17.5 GPa, as shown in Table 2. This difference may be explained by the oxidation conditions conducted in each work as being different. All these works, showed in Table 2, obtained the oxide iron by means of steel oxidation and report more than one layer (magnetite and hematite), except Glasscock et al.<sup>23</sup> who deposited pure hematite on top of a silicon substrate.

Zambrano et al.<sup>24</sup> suggest that this difference in hardness measures may be due to the porosity in the oxide layers and the oxide phases mixture in the same layer. McCarty et al.<sup>27</sup> pointed that the magnetite oxidation can nucleate hematite inclusions. Initially the inclusions are

**Table 2.** Hardness values of hematite and magnetite report by a few authors.

Oxide/ Hardness (GPa)	Fe <sub>2</sub> O <sub>3</sub>	Fe <sub>3</sub> O <sub>4</sub>
Glasscock et al. <sup>23</sup>	17.5	-
Zambrano et al. <sup>24</sup>	12.0	6.5
Arabnejad et al. <sup>25</sup>	5.88	6.67
Takeda et al. <sup>26</sup>	6,70	4.00

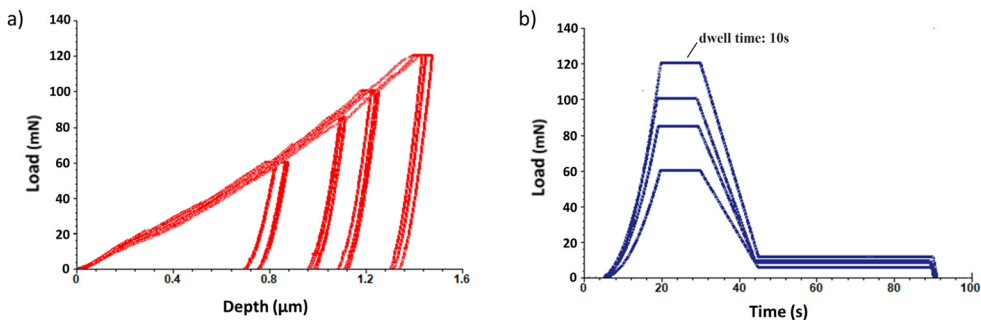


**Figure 7.** Load-displacement curves obtained from nanoindentation measurements on oxidized sample: a) Load-displacement curves; b) dwell time at maximum applied load.

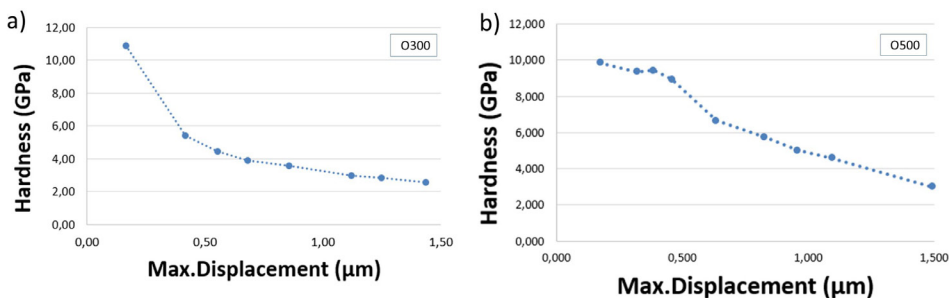


**Figure 8.** Surface hardness results of oxide layers obtained through Berkovich diamond nanoindenter: a) samples O300-2h and b) samples O500-0.5h.

isolated, then eventually the surface is covered by hematite and there are crystalline planes where magnetite turns into hematite faster. As the conditions and oxidation processes of the works presented in Table 2 are different, it is possible that the portion of hematite formed is different, which may explain the different results in hardness measurements.

Current results are within the range found in the literature and are corresponding to the hardness of hematite/magnetite phases mixture in the oxide layer. The fact that the hardness is less than pure hematite hardness reported by Glasscock et al.<sup>23</sup> agrees to the Raman and XRD analyses, that present a non-pure hematite phase. When the magnetite turns completely into hematite there is a difficulty to maintain the layer cohesion. The use of ABiPPS technology enables more flexible control of the energy supplied to the surface by controlling the intensity of high-voltage pulses and the period of low-intensity voltage. In this way it may be possible the control of oxidation process, to achieve different proportion of oxide phases.

Stevenson et al.<sup>28</sup> show that the microhardness of single crystal hematite  $Fe_2O_3$  is highly anisotropy due to the multiple slip systems of the material. Steel oxidation through plasma ABiPPS, may favor a preferential growing direction of oxide layer, depending on the energy of ion and electron bombardment during the process. Therefore, it is necessary further investigation in order to better understand the Young's Modulus and the Hardness in oxide layer obtained through plasma ABiPPS.

Figure 9 shows the Vickers micro-hardness profiles, through the cross-section, for O300-2h and O500-0.5h samples. The applied load was 98 mN (0.01HV) during 10 s. Each point on the graph is a result of three measures average. The hardness profiles show constant values for depth larger than about  $10\mu m$ , which indicates that the oxidation didn't reach the bulk in a significant way. The in-depth hardness distribution is usually monotonously decreasing from the treated surface. This monotonously decreasing is observed only for O500-0.5h sample. It is not observed for O300-2h samples because the Vickers indentation dimensions are larger than the oxide layer thickness, which makes measurement on the layer impracticable. In its turn, the O500-0.5h sample shown similar hardness values, on the oxide layer, for both measurements methods displayed in Figure 8b and Figure 9, namely between 8 and 10 GPa (815 - 1020 HV).

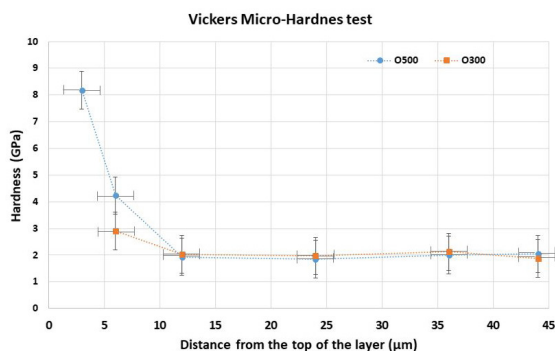


**Figure 9.** Vickers Micro-Hardness profiles on the cross-section of O300 and O500 samples.

## 4. Conclusion

The goal of present paper has been successfully achieved: the oxidation of AISI 1006 steel surface through the 'Asymmetric Bipolar Pulsed Plasma' (ABiPPS) process demonstrates that the ABiPPS technique is viable for the growth of oxide layers on metal surfaces. High energy bipolar pulsed voltage produces sequential bombardment through ions and electrons on the surface, during the oxidation process. The interspersed bombardment can relieve the residual stress in the oxide layer, avoiding its spalling and de-cohesion from the substrate. Results of AISI 1006 steel oxidation show the growth of homogeneous and thick oxide layer in a short treatment time and low temperature:  $6\mu m$  thickness for treatment during 0.5h at  $500^{\circ}C$  and  $1\mu m$  for 2h at  $300^{\circ}C$ . Oxides produced in both temperatures were a mixture of crystalline phases, composed by magnetite and hematite. Hardness of resulting oxide layers were  $11.0\pm 0.2$  GPa for samples treated at  $300^{\circ}C$ , and  $9.6\pm 0.2$  GPa for samples treated at  $500^{\circ}C$ .

## 5. Acknowledgment

This work was supported by the CAPES- Brazil (Finance Code 001), Projeto PRONEM FAPESC-CNPq - 2020TR730 and PROMOP. The authors would like to thank Dr. Evaldo José Corat - LabRam/INPE for Raman analysis.

## 6. References

- Gareth S. Parkinson, iron oxide surfaces. *Surface Science Reports*, 2016;71(1):272-365. <https://doi.org/10.1016/j.surfrep.2016.02.001>.
- Shokrollahi H. A review of the magnetic properties, synthesis methods and applications of maghemite. *J Magn Magn Mater*. 2017;426:74-81. <https://doi.org/10.1016/j.jmmm.2016.11.033>.
- Mitchell TE, Voss DA, Butler EP. The observation of stress effects during the high temperature oxidation of iron. *J Mater Sci*. 1982;17(6):1825-33. <https://doi.org/10.1007/BF00540812>.
- Rhines FN, Wolf JS. The role of oxide microstructure and growth stresses in the high-temperature scaling of nickel. *Metall Mater Trans, B, Process Metall Mater Proc Sci*. 1970;1:1701-10. <https://doi.org/10.1007/BF02642020>.
- Clarke DR. The lateral growth strain accompanying the formation of a thermally grown oxide. *Acta Materialia*, 2003;51(5):1393-407. [https://doi.org/10.1016/S1359-6454\(02\)00532-3](https://doi.org/10.1016/S1359-6454(02)00532-3).
- Panicaud B, Grosseau-Poussard JL, Dinhut JF. On the growth strain origin and stress evolution prediction during oxidation of metals. *Appl Surf Sci*. 2006;252(16):5700-13. <http://dx.doi.org/10.1016/j.apsusc.2005.07.075>.
- Lu X, Mohedano M, Blawert C, Matykina E, Arrabal R, Kainer KU, Zheludkevich ML. Plasma electrolytic oxidation coatings with particle additions – A review. *Surf Coat Tech*. 2016;307(Pt C):1165-82. <http://dx.doi.org/10.1016/j.surfcoat.2016.08.055>.
- Schennach R, Grady T, Naugle DG, Parga JR, McWhinney H, Cocks DL. Plasma oxidation as a tool to design oxide films at low temperatures. *J Vac Sci Technol A*. 2001;19(4):1965-70. <https://doi.org/10.1116/1.1380718>.
- Zhao L, Wei Y, Zhang R, Peng Y. Controlled surface oxidation of HfSe2 via oxygen-plasma treatment. *Mater Lett*. 2019;243:96-9. <http://dx.doi.org/10.1016/j.matlet.2019.02.024>.
- Hrach R, Vicher M, Hrachová V. Study of plasma oxidation of metals. *Vacuum*. 1998;50(1-2):171-3. [http://dx.doi.org/10.1016/S0042-207X\(98\)00040-2](http://dx.doi.org/10.1016/S0042-207X(98)00040-2).

11. Scholtz JS, Fontana LC, Mezaroba M. Asymmetric bipolar plasma power supply to increase the secondary electrons emission in capacitive coupling plasmas. *IEEE Trans Plasma Sci.* 2018;46(8):2999-3007. <http://dx.doi.org/10.1109/TPS.2018.2851071>.
12. Berg M, Budtz-Jørgensen CV, Reitz H, Schweitz KO, Chevallier J, Kringhøj P, Böttiger J. On plasma nitriding of steels. *Surf Coat Technol.* 2000;124(1):25-31. [http://dx.doi.org/10.1016/S0257-8972\(99\)00472-7](http://dx.doi.org/10.1016/S0257-8972(99)00472-7).
13. Arumainayagam CR, Lee H-L, Nelson RB, Haines DR, Gunawardane RP. Low-energy electron-induced reactions in condensed matter. *Surface Science Reports.* 2010;65(1):1-44. <http://doi.org/10.1016/j.surfrep.2009.09.001>.
14. Xu J, Choyke WJ, Yates JT Jr. Enhanced silicon oxide film growth on Si (100) using electron impact. *J Appl Phys.* 1997;82(12):6289-92.
15. Shin H, Zhu W, Xu L, Donnelly VM, Economou DJ. Control of ion energy distributions using a pulsed plasma with synchronous bias on a boundary electrode. *Plasma Sources Sci Technol.* 2011;20(5):055001. <http://doi.org/10.1088/0963-0252/20/5/055001>.
16. Tier MA, Kieckow F, Strohaecker TR, da Silva Rocha A, Bell T. A Study of carbon redistribution during plasma nitriding of steel. *Proceedings of the 15th IFHTSE* 25. 2006:192-8
17. Mos YM, Vermeulen AC, Buisman CJN, Weijma J. X-ray diffraction of iron containing samples: the importance of a suitable configuration. *Geomicrobiol J.* 2018;35(6):511-7. <https://doi.org/10.1080/01490451.2017.1401183>.
18. Everall NJ. Confocal Raman microscopy: performance, pitfalls, and best practice. *Applied Spectrosc.* 2009;63(9):245A-62A.
19. Jonsson T, Pujilaksono B, Hallström S, Ågren J, Svensson J-E, Johansson L-G, Halvarsson M. An ESEM in situ investigation of the influence of H<sub>2</sub>O on iron oxidation at 500°C. *Corrosion Science.* 2009;51(9):1914-24. <https://doi.org/10.1016/j.corsci.2009.05.016>.
20. Oliver WC, Pharr GM. An improved technique for determining hardness and elastic modulus using load and displacement sensing indentation experiments. *J Mater Res.* 1992;7(6):1564-83. <https://doi.org/10.1557/JMR.1992.1564>.
21. International Organization for Standardization. ISO 14577:2015: Metallic materials — Instrumented indentation test for hardness and materials parameters — Part 1: Test method. Geneva: ISO; 2015.
22. Manika I, Maniks J. Effect of substrate hardness and film structure on indentation depth criteria for film hardness testing. *J Phys D Appl Phys.* 2008;41(7):074010. <https://doi.org/10.1088/0022-3727/41/7/074010>.
23. Glasscock JA, Barnes PRF, Plumb IC, Bendavid A, Martin PJ. Structural, optical and electrical properties of undoped polycrystalline hematite thin films produced using filtered arc deposition. *Thin Solid Films.* 2008;516(8):1716-24. <https://doi.org/10.1016/j.tsf.2007.05.020>.
24. Zambrano OA, Coronado JJ, Rodríguez SA. Mechanical properties and phases determination of low carbon steel oxide scales formed at 1200°C in air. *Surf Coat Tech.* 2015;282:155-62. <https://doi.org/10.1016/j.surfcoat.2015.10.028>.
25. Arabnejad H, Shirazi SA, McLaury BS, Subramani HJ, Rhyne LD. The effect of erodent particle hardness on the erosion of stainless steel. *Wear.* 2015;332-333:1098-103. <https://doi.org/10.1016/j.wear.2015.01.017>.
26. Takeda M, Onishi T, Nakakubo S, Fujimoto S. Physical properties of iron-oxide scales on Si-containing steels at high temperature. *Mater Trans.* 2009;50(9):2242-6. <https://doi.org/10.2320/matertrans.M2009097>.
27. McCarty KF, Monti M, Nie S, Siegel DA, Starodub E, El Gabaly F, et al. Oxidation of magnetite (100) to hematite observed by in situ spectroscopy and microscopy. *J Phys Chem C.* 2014;118(34):19768-77. <https://doi.org/10.1021/jp5037603>.
28. Stevenson ME, Kaji M, Bradt RC. Microhardness anisotropy and the indentation size effect on the basal plane of single crystal hematite. *J Eur Ceram Soc.* 2002;22(7):1137-48. [https://doi.org/10.1016/S0955-2219\(01\)00415-0](https://doi.org/10.1016/S0955-2219(01)00415-0).